JOURNAL OF GUIDANCE, CONTROL, AND DYNAMICS
Vol. 26, No. 5, September–October 2003

Analysis of Frozen Conditions and Optimal Frozen Orbit Insertion

M. Aorpimai*
Mahanakorn University of Technology, Bangkok 10530, Thailand
and
P. L. Palmer†
University of Surrey, Guildford, England GU2 7XH, United Kingdom

The frozen conditions of the orbits of Earth satellites are analyzed using a redundant set of elements, called epicycle elements. As well as avoiding the circular orbit singularity, working through the epicycle elements allows the higher geopotential harmonics to be included in the analytic computation up to an arbitrary number of terms until a satisfactory accuracy is achieved. This is important especially for orbits that are close to the critical inclination of 63.4 deg. An optimal single-burn strategy is analyzed for maneuvering a satellite from arbitrary initial conditions toward frozen conditions. It is shown that, while the orbital elements are varying, the minimum delta-*V* requirement will not vary with time. An optimal strategy is proposed for the frozen orbit transfer by using multiple small impulsive burns, which are preferred for modern autonomous orbit operations on small satellites. It is shown that the total delta-*V* required by a series of small burns in the strategy is not greater than the minimum value required by the optimal single-burn strategy. This strategy is examined through the maneuvering of the UoSAT-12, a 300-kg minisatellite, toward frozen conditions by using its low-cost cold-gas thrusters.

Introduction

UNDER frozen conditions, the variations of eccentricity and argument of perigee due to the oblateness of the Earth become zero. The orbital shape of an Earth satellite's orbit is, therefore, preserved at all times, and the satellite altitude variation is minimized. This poses a great advantage to Earth-observation satellites that require minimal variations in altitude when the satellite flies over any particular spot on the ground. There are a number of existing Earth-observation satellites that have been placed into frozen orbits, such as SEASAT,[1] LANDSAT,[‡] SPOT,[§] RADARSAT,[¶] and TOPEX/Poseidon.[**] Some Earth-like missions, such as Martian, Venusian, and lunar orbiters,[2–4] also take advantage of frozen orbits.

In the evaluation of frozen conditions, clear understanding of perturbations due to the nonspherical Earth is required. Existence of the frozen orbit is typically attributed to the balancing of the secular perturbations of the even zonal harmonics with the long-periodic perturbations of the odd zonal harmonics. Early treatments obtained an analytic solution from the second and third zonal harmonic coefficients (J_2 and J_3) which was then extended to higher terms via numerical integration of the mean elements.[5–9] From a more abstract perspective, frozen orbits arise from bifurcations.[10,11] The analytic solution for frozen conditions derived by Coffee et al.,[11] however, only includes the zonal geopotential harmonics up to J_9, whereas the analytic frozen solution successfully derived by Cook[12] uses an arbitrary number of terms in geopotential expansion.

In this paper, we present an analytic solution for frozen conditions without any limitation in the number of zonal harmonics. The analysis is based on the epicycle description, which, as well as avoiding the circular orbit singularity, also permits us in clear and simple geometry to determine the firing strategy and the delta-*V* required to achieve frozen conditions.

In the second part of this paper, we investigate the optimal strategy for maneuvering a satellite from an initial condition to a frozen orbit. Traditionally, a ground-based strategy is employed in maneuvering of a satellite, and it generally requires rich mission resources. The orbit maneuver of TOPEX/Poseidon,[13] for example, uses satellite laser ranging and Doppler orbitography and radiopositioning integrated by satellite data to create precise orbit ephemerides for the orbit determination system.[14] A monopropellant hydrazine blowdown propulsion system consisting of 12, 1-N and 4, 22-N thrusters is used for orbit and attitude control. In a low-cost small satellite mission, however, the resources available for both the onboard and ground segments are limited. Their orbit determination and control units, for instance, rely on some standard components for small satellites, such as an onboard global positioning system receivers and chemical low-thrust propulsion systems.

The strategy we present in this paper is aimed for low-thrust firing suitable for autonomous orbit maneuvering. This strategy employs a series of small burns in the in-plane direction instead of a small number of large burns. We prove that the total delta-*V* required for our strategy is not greater than the optimal dual-firing strategy analyzed by Jones.[15] The proposed method is demonstrated through the UoSAT-12, a 300-kg Earth-observation satellite.[16]

In the next section, we introduce a simple analysis of the frozen orbit conditions where only J_2 and J_3 harmonics are included. We then present a more elaborate analysis based on the epicycle orbit description where an arbitrary number of terms in the potential harmonics can be included. Then, we propose optimal orbit maneuvers that will place a satellite into frozen orbit. Finally, we demonstrate the strategy through the numerical simulation of a specific satellite, the UoSAT-12.

Frozen Orbits Analysis

The term frozen orbit was first introduced in 1978 by Cutting et al. in their work on the analysis of the SEASAT-A orbit.[1] The analysis of such stable conditions, however, had originally been developed by Cook[12] in 1966.

Consider the simplest case for frozen conditions where only first order in J_2 and J_3 harmonics are taken into account. The averaged variational rate equations for eccentricity and argument of perigee

Received 9 March 2001; revision received 26 March 2003; accepted for publication 26 March 2003.

*Lecturer, Small Satellite Research Centre.
†Senior Lecturer, Surrey Space Centre.

‡Data available online at http://1s7pm3.gsfc.nasa.gov [cited 1 March 2003].

§Data available online at http://www.spotimage.fr [cited 1 March 2003].

¶Data available online at http://radarsat.space.gc.ca [cited 1 March 2003].

**Data available online at http://topex-www.jpl.nasa.gov [cited 1 March 2003].

for an Earth model consisting of zonal harmonics J_2 and J_3 can be expressed as[1]

$$\frac{de}{dt} = \frac{-3J_3 n}{2(1-e^2)^2}\left(\frac{R_e}{a}\right)^3 \sin I_0\left(1-\frac{5}{4}\sin^2 I_0\right)\cos\omega \quad (1)$$

$$\frac{d\omega}{dt} = \frac{3J_2 n}{(1-e^2)^2}\left(\frac{R_e}{a}\right)^2\left(1-\frac{5}{4}\sin^2 I_0\right)F \quad (2)$$

where

$$F = 1 + \frac{J_3}{2J_2(1-e^2)}\left(\frac{R}{a}\right)\left(\frac{\sin^2 I_0 - e^2\cos^2 I_0}{\sin I_0}\right)\frac{\sin\omega}{e}$$

These equations show secular and long-period variations in terms of mean orbital elements, namely, semimajor axis a, eccentricity e, inclination I_0, and argument of perigee ω. R_e is the Earth's mean radius at the equator, and n is the mean motion.

Note that there is no J_2 term in Eq. (1) but that Eq. (2) contains both J_2 and J_3. Also note that both equations contain the factor $[1-(5/4)\sin^2 I_0]$. This expression equals zero when $I_0 = 63.4$ deg (or $I_0 = 116.6$ deg), the critical inclination. At this inclination, both eccentricity and argument of perigee remain constant. The notorious Molniya orbit employs these conditions to control passively its elongated orbital shape to be fixed in inertial space.

However, for given values of mean semimajor axis and inclination, to this level of approximation, the variation in eccentricity can also be stopped by choosing the argument of perigee to be either 90 or 270 deg. The argument of perigee rotation rate can then be nullified by setting F in Eq. (2) to be zero. To first order in both zonal harmonic coefficients and eccentricity, the required eccentricity is approximately

$$e = -(J_3/2J_2)(R_e/a)\sin I_0 \quad (3)$$

This is a very small eccentricity, $\mathcal{O}(10^{-3})$, which shows that the balancing of the secular and long-periodic perturbations can be satisfied by near circular orbits when the inclination is not close to critical. These conditions are referred to as frozen conditions, and the eccentricity and argument of perigee for $de/dt = 0$ and $d\omega/dt = 0$ are referred to as frozen eccentricity and frozen argument of perigee, respectively.

Orbital Dynamics

Epicycle Description

The description of the near-circular motion of a satellite under an axisymmetric potential can be summarized through a linearized set of equations called epicycle equations.[17] Like other nonsingular elements, the epicycle elements are introduced in such a way that terms that have a small divisor of e are removed. Although the epicycle description has a simple geometric interpretation and greater mathematical simplicity than conventional descriptions, it is sufficiently accurate to describe the motion of a satellite over its lifetime.

The idea is based on using two polar coordinates (Fig. 1), radial r and azimuthal angle λ (argument of latitude), and two orbital elements, inclination I and ascending node Ω, which complete four redundant coordinates to describe the location of a satellite S at any time. The evolution of these quantities in time is given by

$$r = a(1+\rho) - A\cos(\alpha - \alpha_P) + a\chi\sin((1+\kappa)\alpha) + \Delta_r \quad (4a)$$

$$\lambda = (1+\kappa)\alpha + (2A/a)[\sin(\alpha-\alpha_P) + \sin\alpha_P] - 2\chi\{1-\cos[(1+\kappa)\alpha]\} + \Delta_\lambda \quad (4b)$$

$$I = I_0 + \Delta_I \quad (4c)$$

$$\Omega = \Omega_0 + \vartheta\alpha + \Delta_\Omega \quad (4d)$$

where $\alpha = nt$ and n is the mean motion. In these equations, a is a mean semimajor axis defined through the conserved orbital energy

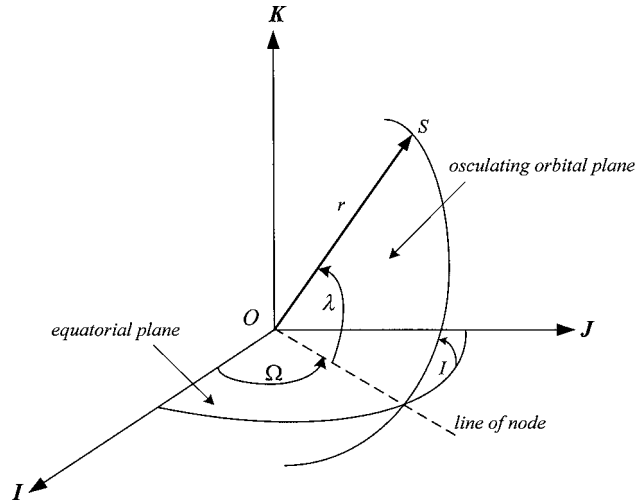

Fig. 1 Coordinate system.

ε when only zonal harmonics are included:

$$a = -(\mu/2\varepsilon) \quad (5)$$

and μ is the gravitational parameter that is related to n through Kepler's law: $a^3 n^2 = \mu$. Time is measured from an initial equator crossing, I_0 and Ω_0 are the osculating inclination and ascending node at $t = 0$, and A and α_P are two integration constants appearing in the derivation of Eqs. (4). We call A the epicycle amplitude.

The constant offset in orbital radius caused by even zonal harmonics is described by ρ. The secular change in the ascending node is described by ϑ, which gives a linear variation of Ω with time. The secular drift in the argument of perigee is described by κ, which causes a drift in the argument of latitude. The long-periodic variations, which are caused by the odd zonal harmonics, are described by χ, and the short-periodic variations are expressed as a Fourier series through the terms Δ_x for each of the four coordinates. When the epicycle phase α changes by 2π, then the argument of latitude changes secularly by an amount $2\pi + 2\kappa\pi$. The argument of latitude can then be considered to vary with time as $\lambda \sim n_N t$, where

$$n_N = (1+\kappa)n \quad (6)$$

and $2\pi/n_N$ is the nodal period.

The closed-form solutions for the secular perturbation terms for an axisymmetric Earth where only first order in zonal geopotential harmonics are taken into account are[17]

$$\rho = \sum_{m=1}\rho_{2m} = \sum_{m=1}(2m-1)J_{2m}\left(\frac{R_e}{a}\right)^{2m} L^0_{2m} \quad (7a)$$

$$\vartheta = \sum_{m=1}\vartheta_{2m} = -\sum_{m=1}2J_{2m}\left(\frac{R_e}{a}\right)^{2m}\frac{\cot I_0}{\sin I_0}\sum_{l=1}^{m} 2l L^{2l}_{2m} \quad (7b)$$

$$\kappa = \sum_{m=1}\kappa_{2m} = -\sum_{m=1}(4m-1)J_{2m}\left(\frac{R_e}{a}\right)^{2m} L^0_{2m} - \vartheta_{2m}\cos I_0 \quad (7c)$$

and the long-period terms are given by

$$\chi = \sum_{m=1}\chi_{2m+1} = -\sum_{m=1}\frac{2m J_{2m+1}}{\kappa}\left(\frac{R_e}{a}\right)^{2m+1} L^1_{2m+1} \quad (8)$$

where $m = 1, 2, 3, \ldots, l = 1, 2, 3, \ldots,$ J_n are the nth deg of the Earth's zonal gravitational harmonic coefficients and the coefficients L^j_i are given by

$$L^j_i = \frac{(i-j)!}{(i+j)!}P^j_i(0)P^j_i(\cos I_0) \quad (9)$$

and P_i^j are the associated Legendre polynomials. Although, in principle, we can take into account higher-order terms as well as higher degree of zonal harmonics in κ for the evaluation of long-periodic terms in Eq. (8), in practice we need only consider the term with J_2 because it is of 10^{-3} order, whereas other terms are of order 10^{-6}. The equation then can be explicitly expressed as

$$\kappa_2 = \tfrac{3}{4} J_2 (R_e/a)^2 \left(4 - 5\sin^2 I_0\right) \tag{10}$$

The short periodic variations caused by J_2 can be found as

$$\Delta_{r2} = \tfrac{1}{4} J_2 a (R_e/a)^2 \sin^2 I_0 \cos 2\alpha \tag{11a}$$

$$\Delta_{\lambda 2} = -\tfrac{1}{8} J_2 (R_e/a)^2 \left(6 - 7\sin^2 I_0\right) \sin 2\alpha \tag{11b}$$

$$\Delta_{I2} = -\tfrac{3}{8} J_2 (R_e/a)^2 \sin 2I_0 (1 - \cos 2\alpha) \tag{11c}$$

$$\Delta_{\Omega 2} = \tfrac{3}{4} J_2 (R_e/a)^2 \cos I_0 \sin 2\alpha \tag{11d}$$

Note that, in the absence of perturbing terms, the epicycle equations reduce to

$$r = a - A\cos(\alpha - \alpha_P) \tag{12a}$$

$$\lambda = \alpha + (2A/a)[\sin(\alpha - \alpha_P) + \sin\alpha_P] \tag{12b}$$

$$I = I_0 \tag{12c}$$

$$\Omega = \Omega_0 \tag{12d}$$

In the two-body case, I and Ω are fixed, and the eccentricity and argument of perigee are also constants related directly to the parameters A and α_P, respectively.

Update Epicycle Parameters

When the satellite's thrusters are fired, the epicycle parameters will change. In this section we shall derive the effect on the epicycle parameters of an arbitrary in-plane impulsive delta-V. When the radial and phase epicycle equations are differentiated with the short-periodic terms excluded and high-order terms in J_n ignored, we obtain the radial and azimuthal velocities as

$$V_r = n[A\sin(\alpha - \alpha_P) + a\chi(1 + \kappa)\cos\beta] \tag{13a}$$

$$V_\lambda = (1 + \kappa) n\{a(1 + \rho) + A[1 + 2(\rho - \kappa)]\cos(\alpha - \alpha_P) - (1 + 2\rho) a\chi \sin\beta\} \tag{13b}$$

where $V_r = \dot{r}$, $V_\lambda = r\dot{\lambda}$, and $\beta = (1 + \kappa)\alpha$. At the instant of firing, the velocity components will change impulsively while the position remains the same. Thus, after firing,

$$\hat{r} = r \tag{14a}$$

$$\hat{\lambda} = \lambda \tag{14b}$$

$$\hat{V}_r = V_r + \Delta V_r \tag{14c}$$

$$\hat{V}_\lambda = V_\lambda + \Delta V_\lambda \tag{14d}$$

where ΔV_r and ΔV_λ are the delta-V components along the radial and azimuthal directions, respectively. The caret over a variable refers to its value after firing. The change in a can be solved from the change in orbital energy $\Delta\varepsilon$:

$$\Delta a = 2\Delta\varepsilon/an^2 = (2/an^2)(V_r \cdot \Delta V_r + V_\lambda \cdot \Delta V_\lambda) \tag{15}$$

which, to first order in J_n, results in

$$\hat{a} = a + (2\Delta V_\lambda/n) \tag{16}$$

By knowing $\hat{a}$ and using the same approximation, we can rearrange the velocity Eqs. (13) and (14) to give

$$\hat{A}\cos(\alpha - \hat{\alpha}_P) = A\cos(\alpha - \alpha_P) + (2\Delta V_\lambda/n) \tag{17a}$$

$$\hat{A}\sin(\alpha - \hat{\alpha}_P) = A\sin(\alpha - \alpha_P) + (\Delta V_r/n) \tag{17b}$$

where $\hat{A}$ and $\hat{\alpha}_P$ are the postfiring variables of the epicycle parameters A and α_P, respectively. These equations can be further rearranged as

$$\Delta\xi\cos\alpha + \Delta\eta\sin\alpha = 2\Delta V_\lambda/n \tag{18a}$$

$$\Delta\xi\sin\alpha - \Delta\eta\cos\alpha = \Delta V_r/n \tag{18b}$$

where $\Delta\xi = \hat{A}\cos\hat{\alpha}_P - A\cos\alpha_P$ and $\Delta\eta = \hat{A}\sin\hat{\alpha}_P - A\sin\alpha_P$. These equations provide the solution for the effect on orbital eccentricity and argument of perigee when firing the thrusters.

Frozen Orbit Conditions as Functions of Epicycle Parameters

The frozen orbit solutions obtained from the simple analysis with only J_2 and J_3 terms included may not be accurate enough in practice, especially for orbits with inclinations close to the critical value. The analysis of frozen orbits through the epicycle parameters allows us to simply include higher terms of zonal harmonics.

In the evaluation of frozen conditions, we consider only secular and long-periodic perturbations. The short-periodic variations, therefore, can be averaged out. Only the variation caused by first order in J_2 is taken into account because its magnitude is approximately 10^3 times larger than other higher terms. The J_2 short-periodic variation can be averaged out by integrating over half an orbital period.

We define the half-orbit average of a quantity $Q(\alpha)$ varying around the orbit as

$$\bar{Q} = \frac{1}{\pi}\int_{\upsilon}^{\upsilon+\pi} Q(\alpha)\,\mathrm{d}\alpha$$

where υ is an arbitrary phase. The in-plane motion in Eq. (4) with the short-periodic variations in Eq. (11) included can be averaged to give

$$\bar{r} = a(1 + \rho) + (2A/\pi)\sin(\upsilon - \alpha_P) + a\chi\cos\beta \tag{19a}$$

$$\bar{\lambda} = \tfrac{1}{2}(1 + \kappa)(\pi + 2\upsilon) + (4A/a\pi)\cos(\upsilon - \alpha_P) + (2A/a)\sin\alpha_P - 2\chi - 2\chi\cos\beta \tag{19b}$$

By setting $\upsilon = \gamma - \pi/2$, Eq. (19) can be rearranged as

$$\bar{r} = a(1 + \rho) - \bar{A}\cos(\gamma - \alpha_P) + a\chi\sin\beta \tag{20a}$$

$$\bar{\lambda} = (1 + \kappa)\gamma + (2\bar{A}/a)[\sin(\gamma - \alpha_P) + \sin\alpha_P] - 2\chi(1 - \cos\beta) + (2/a)(A - \bar{A})\sin\alpha_P \tag{20b}$$

where $\bar{A} = 2A/\pi$. Both the radial and azimuthal equations are now formally identical to Eqs. (4) but without the short-periodic terms. In the azimuthal equation, there is the addition of a constant term. Equations (20) can be further rearranged by combining the epicycle and long-periodic terms as

$$\bar{r} = a(1 + \rho) - G\cos(\gamma - \omega) \tag{21a}$$

$$a\bar{\lambda} = (1 + \kappa)\gamma - (2G/a)[\sin(\gamma - \omega) + \sin\omega] + \bar{\lambda}_0 \tag{21b}$$

where $\bar{\lambda}_0 = (2A/a)\sin\alpha_P - 2\chi$ and G and ω relate to $\bar{A}$ and α_P through

$$G\cos\omega = \bar{A}\cos(\alpha_P + \kappa\gamma) \tag{22a}$$

$$G\sin\omega = \bar{A}\sin(\alpha_P + \kappa\gamma) + a\chi \tag{22b}$$

We have now formulated the averaged perturbed in-plane equations of motion to give forms equivalent to the two-body equations (12). The eccentricity and argument of perigee are represented

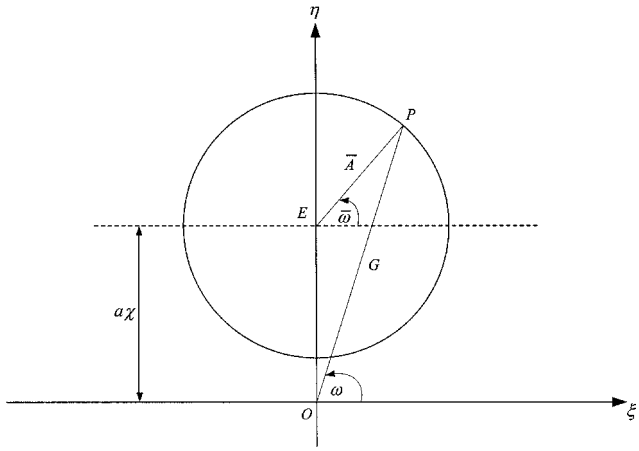

Fig. 2 Orientation of G and ω, orientation of eccentricity and argument of perigee, respectively, around the frozen conditions.

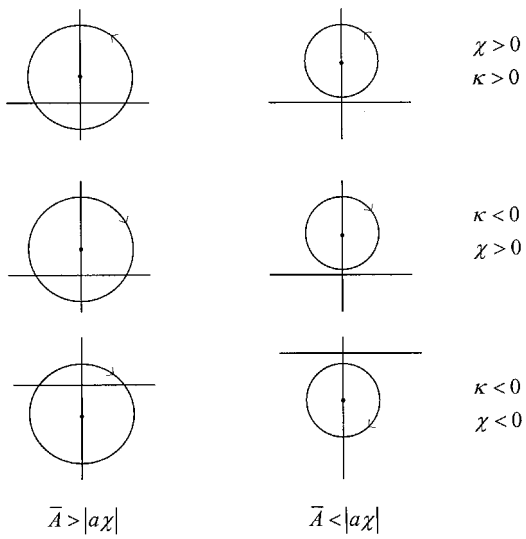

Fig. 3 Rotation modes of the eccentricity vector.

through G and ω, respectively, which now vary with time in inertial space. The evolution of the eccentricity vector is shown in Fig. 2 in the $[\xi, \eta]$ plane, where $\xi = G\cos\omega$ and $\eta = G\sin\omega$. The evolution is circular around a constant point fixed in inertial space (marked by the point E). The center of the circle is defined by the long-periodic perturbation term, χ, and is located at $[0, a\chi]$. The radius of the circle is defined by the epicycle radius, and $\bar{A}\cdot\omega \cong \alpha_p + \kappa\gamma$ defines an instantaneous state. The rotation rate around the circle is κn. Note that, at least to this level of approximation, whereas the circle center and rotation frequency depend on the long-periodic and secular perturbation effects, respectively, the radius of the circle is not a function of any geopotential perturbation terms.

As shown in Fig. 2, the eccentricity and argument of perigee oscillate around a stable point E. However, if the radius of the circle is greater than the line $\overline{OE}$, then ω appears to rotate through 360 deg rather than librate abound 90 deg. From the preceding discussion the motion modes of the eccentricity vector can be summarized in Fig. 3. Whereas the sign of κ affects the direction of the motion, the magnitude of χ defines whether the argument of perigee will be rotating or librating around the frozen value.

In the case where the initial conditions are exactly at point E, the eccentricity vector is frozen. The frozen eccentricity and frozen argument of perigee can be defined through $G\cos\omega = 0$ and $G\sin\omega = a\chi$. The first equation fixes $\omega = 90$ or -90 deg, and hence,

$$G = \pm a\chi \tag{23}$$

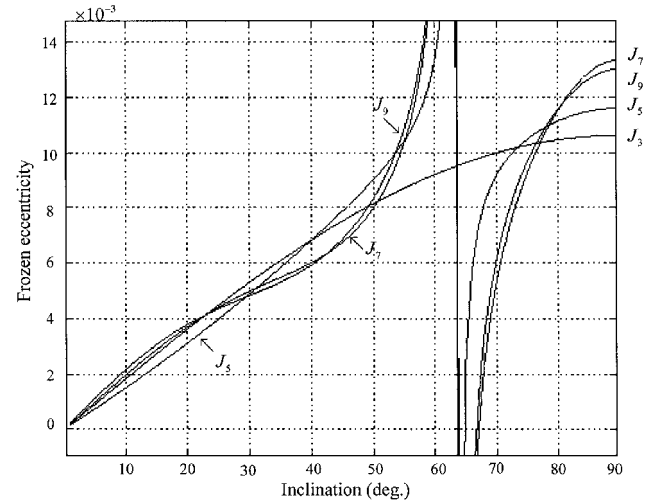

Fig. 4 Frozen eccentricity as function of orbital inclination at $a = 7028$ km; vertical line marks critical inclination 63.4 deg.

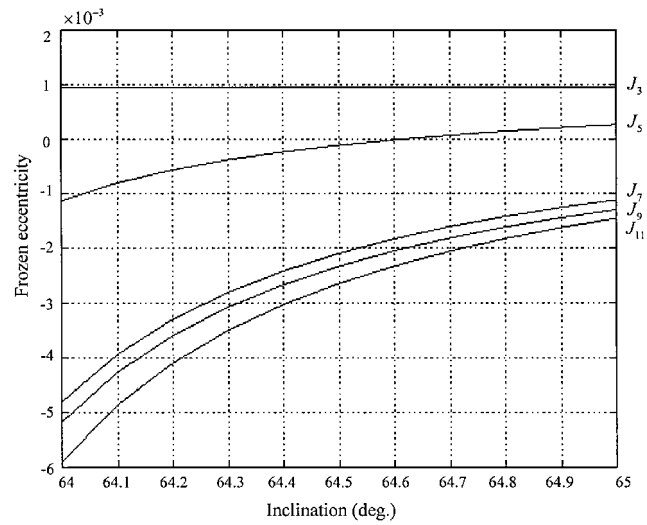

Fig. 5 Frozen eccentricities at inclinations around 64.57 deg; various solutions when terms up to J_{11} are included in the computation of χ.

The frozen orbit solution is a function of orbital inclination and radius. Figure 4 shows the frozen eccentricity against inclination for an epicycle radius of $a = 7028$ km. The different frozen solutions when different odd zonal harmonics are included are also shown in Fig. 4. We can see that the frozen eccentricity does not vary significantly at low inclinations, but there are large variations as the orbital inclination approaches criticality. This suggests that higher terms than J_3 are needed to evaluate the frozen orbit solution, especially in the vicinity of the critical inclination. These results are similar to Cook's[2] when terms up to J_9 were included. Figure 5 shows the frozen eccentricity for some inclinations around $I_0 = 64.57$ deg. (This is the operational inclination of the UoSAT-12, which will be used for the demonstration in the next sections.) The negative sign suggests that the frozen argument of perigee at these inclinations is at $\omega = -90$ deg. At $I_0 = 64.57$ deg, odd zonal harmonics up to J_{25} may be required for the evaluation of a frozen orbit as shown in Fig. 6.

Optimal Transfer to Frozen Orbit

Optimal Single-Burn Strategy

After evaluating the frozen orbit conditions for a satellite in a near-circular orbit, we now determine the optimal strategy for maneuvering a satellite from its initial orbit into frozen orbit. We may treat Fig. 2 as a vector addition problem. The eccentricity vector of an orbit at some instant is represented by $\overline{OP}$ and needs

to be changed to $\overline{OE}$ for frozen conditions. Therefore, we need to add the vector $\overline{PE}$ as the result of an orbit maneuver. To preserve the semimajor axis and inclination, a dual-firing strategy can be employed for generating such an eccentricity vector change, and the delta-V requirement and phase for firing may be found in Ref. 15.

In general, the frozen solution is more sensitive to the change in inclination than the change in orbital size. We can see from Fig. 5 that, at an orbit around $a = 7028$ km and $I_0 = 64.57$ deg, only 0.1-deg change in inclination can cause the difference in frozen eccentricity up to 0.001, whereas, in Fig. 7, it changes less than 1×10^{-5} for 10-km change in semimajor axis. With the orbital inclination assigned, in principle, one can transfer a satellite orbit toward frozen conditions by applying only a single in-plane firing to change its eccentricity vector. However, the single-burn strategy can be useful only when the difference between the initial conditions of the satellite orbit and the frozen conditions is not too large and the effect on the frozen conditions of the change in semimajor axis after the firing can be neglected. The change in semimajor axis for some missions, however, may be unacceptable, for example, those missions that require exact repeat groundtrack. In such a case, a dual-firing strategy may be employed.

The delta-V vector required for the single-burn strategy varies according to the firing phase. The changes $\Delta\xi$ and $\Delta\eta$ required to put the satellite into frozen orbit determine directly the thrust vector required from Eq. (18). The resulting thrust vector is clearly a function of the orbital phase α. We can see from Fig. 8 how the in-plane delta-V components, as well as the total delta-V magnitude required for changing to frozen conditions, vary with the epicycle phase of firing.

Let us introduce a cost function to be minimized as

$$J = (2/n)\sqrt{(\Delta V_\lambda)^2 + (\Delta V_r)^2} \tag{24}$$

Substituting Eq. (18) into the cost function and rearranging the equation, we obtain

$$J = 2\sqrt{\left[\left(\tfrac{1}{4}\right)\Delta\eta^2 + \Delta\xi^2\right]\sin^2\alpha + \left[\left(\tfrac{1}{4}\right)\Delta\xi^2 + \Delta\eta^2\right]\cos^2\alpha - \left(\tfrac{3}{2}\right)\Delta\eta\Delta\xi\sin\alpha\cos\alpha} \tag{25}$$

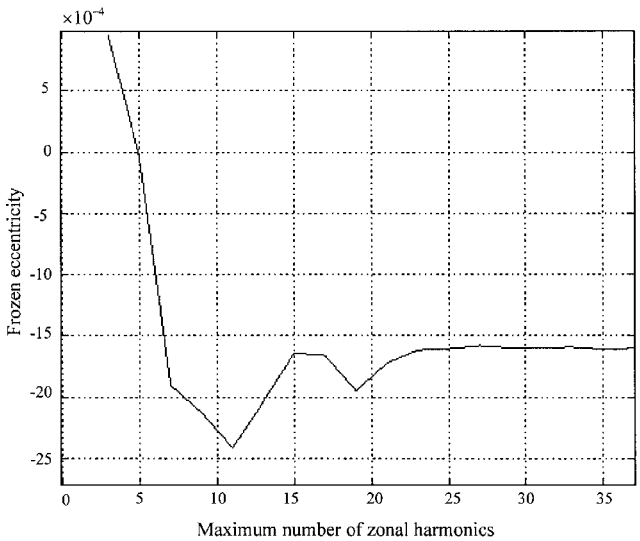

Fig. 6 Convergence of the frozen eccentricity solution as more odd zonal harmonics are included in χ, for an inclination of 64.57 deg.

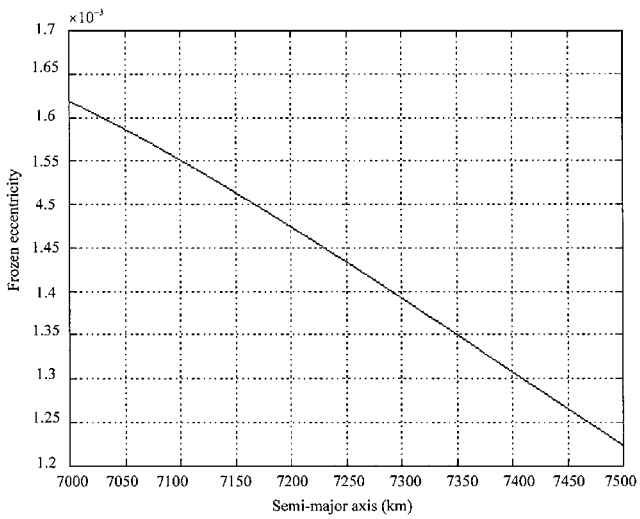

Fig. 7 Frozen eccentricity as a function of altitude.

Minimizing this cost function with respect to the epicycle phase α, we obtain $(\Delta\xi^2 - \Delta\eta^2)\sin\alpha\cos\alpha - \Delta\eta\Delta\xi(\cos^2\alpha - \sin^2\alpha) = 0$, which can be rearranged to give the optimal firing phase α_{opt} as

$$\tan 2\alpha_{\text{opt}} = \frac{2\Delta\eta\Delta\xi}{\Delta\xi^2 - \Delta\eta^2} \tag{26}$$

To satisfy the optimal condition in Eq. (26), we can set

$$\Delta\eta = C\sin\alpha_{\text{opt}} \tag{27a}$$

$$\Delta\xi = C\cos\alpha_{\text{opt}} \tag{27b}$$

where C is a constant.

Substituting Eq. (27) back into (25), we obtain the minimum cost function

$$J_{\min} = 2\sqrt{\tfrac{1}{2}C^2(\sin^4\alpha + \cos^4\alpha + 2\sin^2\alpha\cos^2\alpha)} = C \tag{28}$$

and, from Eq. (27),

$$J_{\min} = \sqrt{\Delta\eta^2 + \Delta\xi^2} \tag{29}$$

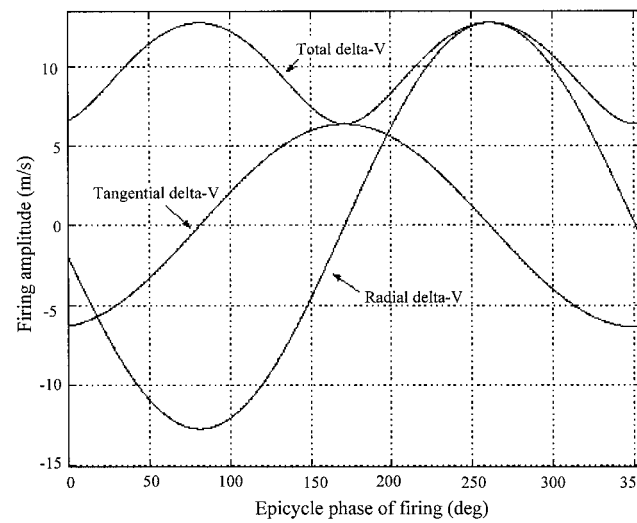

Fig. 8 Variation of delta-V components and total delta-V magnitude at different firing phases using single-burn strategy.

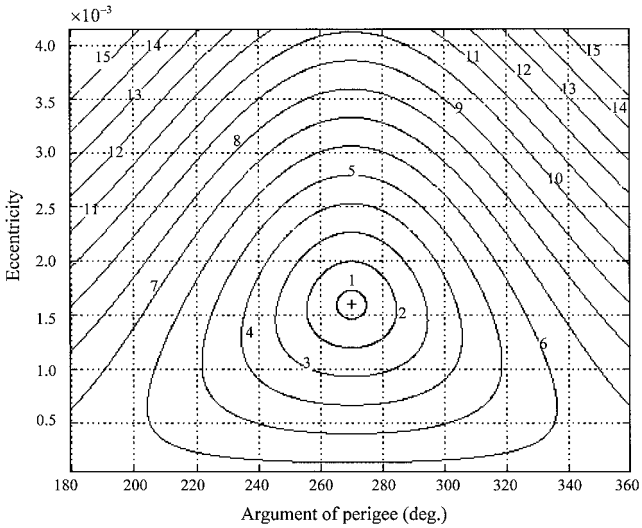

Fig. 9 Orientations of mean eccentricity and argument of perigee at the operational orbit of $a = 7028$ km and $I_0 = 64.57$ deg; numbers are minimum delta-V requirements in meters/second for maneuvering the orbit at any point along the contour toward the frozen conditions.

The delta-V magnitude relates to the cost function through

$$\Delta V = (n/2)J \tag{30}$$

The minimum delta-V magnitude required at the optimum firing phase is

$$\Delta V_{\min} = (n/2)\sqrt{\Delta\eta^2 + \Delta\xi^2} \tag{31}$$

Under frozen conditions, $\cos\omega = 0$. The minimum delta-V requirement can then be formulated in terms of initial $[e_i, \omega_i]$ and final $[e_f, \omega_f]$ conditions as

$$\Delta V_{\min} = (v/2)\sqrt{e_i^2 + e_f^2 - 2e_i e_f \sin\omega_i} \tag{32}$$

where v is the along-track velocity.

From Fig. 2 we can see that to transfer a satellite from any initial conditions along the contour to the frozen conditions requires the same magnitude of change in the $[\xi, \eta]$ plane. Equation (31) shows that the minimum delta-V is also proportional to this quantity for an epicycle orbit. Therefore, under a zonal geogravitational disturbance force, the minimum delta-V required for frozen orbit transfer will not vary with time. The $[e, \omega]$ contour is equivalent to the contour of minimum delta-V requirement as shown in Fig. 9. The numbers labeled on each contour is the minimum delta-V requirement in meters per second for maneuvering the orbit at any point along the contour toward the frozen conditions. Note that, although the argument of perigee evolves secularly for some orbits in Fig. 9, the eccentricity varies in such a way that the delta-V requirement is the same even when ω reaches the frozen value. Also note that, at the optimal firing phase, the required radial delta-V component is zero and that the delta-V required is purely in the along-track direction. This can be easily seen by substituting Eq. (27) into Eq. (18), or from Fig. 8.

Optimal Multiple-Burns Strategy

The problem of small satellites is that they have limited capacity in their propulsion systems. To transfer a small satellite into a frozen orbit by using the optimal single-burn strategy described is generally not possible if the initial conditions are not particularly close to the frozen state. Instead, a series of small burns can be used to move a satellite gradually toward frozen conditions. Figure 10 shows the effect of a single small thruster burn.

With a fixed delta-V capacity, at each step the magnitude and direction of the eccentricity change varies with the delta-V direction

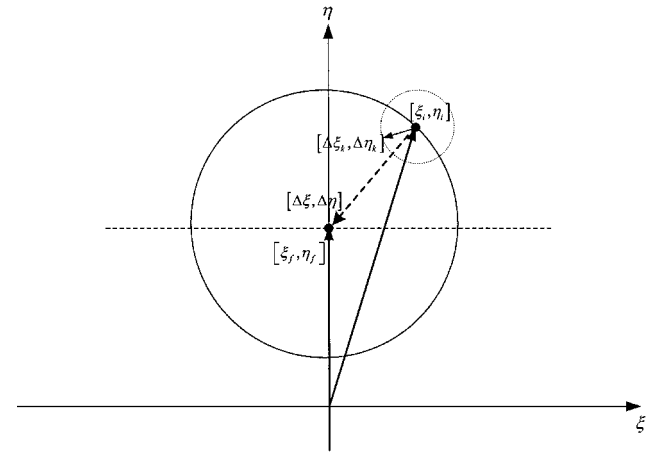

Fig. 10 Geometry of the multiple-burn strategy.

and firing phase. To use each small burn most effectively for maneuvering the orbit toward frozen conditions, the delta-V should be fired so that the eccentricity vector changes in the steepest descent toward the target conditions. From Eq. (18), the changes in epicycle parameters $\Delta\xi$ and $\Delta\eta$ resulting from a given delta-V are

$$\Delta\xi = (2\Delta V_\lambda/n)\cos\alpha + (\Delta V_r/n)\sin\alpha \tag{33a}$$

$$\Delta\eta = (2\Delta V_\lambda/n)\sin\alpha - (\Delta V_r/n)\cos\alpha \tag{33b}$$

The cost function for the optimization problem can be introduced as the dot product between the required eccentricity vector change and the actual change according to a small impulsive delta-V. The fixed delta-V magnitude is also adjoined into the cost function as a constraint:

$$J = \Delta\eta_{fk} \cdot \Delta\eta_k + \Delta\xi_{fk} \cdot \Delta\xi_k + \lambda_V\left(\Delta V_\lambda^2 + \Delta V_r^2 - \Delta V^2\right) \tag{34}$$

where λ_V is the Lagrange multiplier, $\Delta\eta_{fk} = \eta_f - \eta_k$, and $\Delta\xi_{fk} = \xi_f - \xi_k$, where η_k and ξ_k are instantaneous states before each firing and $\Delta\eta_k$ and $\Delta\xi_k$ are the predicted changes. Substituting Eqs. (33) into (34), we obtain the cost function as a function of delta-V components and firing phase:

$$\begin{aligned} J = {} & \Delta\eta_{fk}[(2\Delta V_\lambda/n)\sin\alpha - (\Delta V_r/n)\cos\alpha] \\ & + \Delta\xi_{fk}[(2\Delta V_\lambda/n)\cos\alpha + (\Delta V_r/n)\sin\alpha] \\ & + \lambda_V\left(\Delta V_\lambda^2 + \Delta V_r^2 - \Delta V^2\right) \end{aligned} \tag{35}$$

By setting the partial derivative of the cost function with respect to each variable to be zero, that is,

$$\frac{\partial J}{\partial\alpha} = \frac{\partial J}{\partial\Delta V_\lambda} = \frac{\partial J}{\partial\Delta V_r} = \frac{\partial J}{\partial\Delta\lambda_v} = 0$$

we obtain a set of four equations to be solved for the optimal firing conditions:

$$\begin{aligned} & \Delta\eta_{fk}[(2\Delta V_\lambda/n)\cos\alpha + (\Delta V_r/n)\sin\alpha] \\ & \quad + \Delta\xi_{fk}[-(2\Delta V_\lambda/n)\sin\alpha + (\Delta V_r/n)\cos\alpha] = 0 \end{aligned} \tag{36}$$

$$\Delta V_\lambda = -(1/n\lambda_V)\left(\Delta\xi_{fk}\cos\alpha + \Delta\eta_{fk}\sin\alpha\right) \tag{37}$$

$$\Delta V_r = -(1/2n\lambda_V)\left(\Delta\xi_{fk}\sin\alpha - \Delta\eta_{fk}\cos\alpha\right) \tag{38}$$

$$\Delta V_\lambda^2 + \Delta V_r^2 = \Delta V^2 \tag{39}$$

Substituting Eqs. (37) and (38) into Eq. (36) and rearranging the resulting equation yields

$$\left(3/2n^2\lambda_V\right)\left[\tfrac{1}{2}\left(\Delta\xi_{fk}^2 - \Delta\eta_{fk}^2\right)\sin 2\alpha - \Delta\eta_{fk}\Delta\xi_{fk}\cos 2\alpha\right] = 0 \tag{40}$$

which can be immediately solved for the optimal firing phase as

$$\tan 2\alpha_{\text{opt}_k} = \frac{2\Delta\eta_{f_k}\Delta\xi_{f_k}}{\Delta\xi_{f_k}^2 - \Delta\eta_{f_k}^2}$$

or

$$\tan\alpha_{\text{opt}_k} = \Delta\eta_{f_k}/\Delta\xi_{f_k} \tag{41}$$

The relations between $\Delta\eta_{f_k}$, $\Delta\xi_{f_k}$ and α_{opt_k} can be found as

$$\Delta\eta_{f_k} = C\sin\alpha_{\text{opt}_k} \tag{42a}$$

$$\Delta\xi_{f_k} = C\cos\alpha_{\text{opt}_k} \tag{42b}$$

where C is a constant. Now substituting Eq. (42) into Eq. (38), we obtain the optimal delta-V components as

$$\Delta V_r = 0 \tag{43}$$

and from Eq. (39)

$$\Delta V_\lambda = \Delta V \tag{44}$$

When the preceding optimal solutions are substituted into Eq. (37), the Lagrange multiplier can be found as a constant:

$$\lambda_V = -(C/n\Delta V) \tag{45}$$

The ratio between the required change in η to ξ is always constant at every firing step. Thus, according to Eq. (41), the optimal firing phase measured from the equator is fixed. To prove this, let us consider the relationship of the changes at a firing step k and its successive step $k+1$:

$$\tan\alpha_{\text{opt}_{k+1}} = \frac{\Delta\eta_{f_{k+1}}}{\Delta\xi_{f_{k+1}}} = \frac{\Delta\eta_{f_k} - \Delta\eta_k}{\Delta\xi_{f_k} - \Delta\xi_k} \tag{46}$$

Substituting Eqs. (42) and (33) with the optimal delta-V components from Eqs. (43) and (44) into Eq. (46), we obtain

$$\tan\alpha_{\text{opt}_{k+1}} = \frac{C\sin\alpha_{\text{opt}_k} - (2\Delta V/n)\sin\alpha_{\text{opt}_k}}{C\cos\alpha_{\text{opt}_k} - (2\Delta V/n)\cos\alpha_{\text{opt}_k}} = \tan\alpha_{\text{opt}_k} \tag{47}$$

Figure 11 shows the states move from arbitrary initial conditions toward the frozen state along a steepest descent path with a fixed epicycle phase at firings. The firing locations along the orbit are approximately fixed in inertial space. All small burns can be thought of as an idealized single impulsive burn to frozen orbit, which would occur at this same inertial position, broken up into small steps to make them executable by a low-thrust spacecraft.

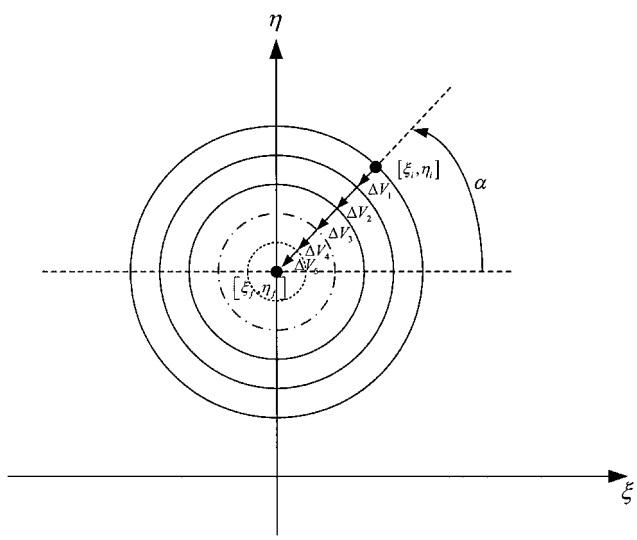

Fig. 11 Optimal firing phase for multiburn strategy.

Frozen Orbit Transfer of UoSAT-12

The study of frozen orbit insertion for UoSAT-12 by using optimal multiple small burns will be given as an example here. The UoSAT-12, a 300-kg minisatellite,[16] was launched into a near-circular orbit at the altitude of approximately 650 km and inclination of 64.57 deg. The spacecraft acceleration when using two cold-gas thrusters is around 1 mm/s^2; thus, if we assume that a burn length of 5 min is the longest that can be approximated as impulsive, taking as it does roughly 18 deg of an orbit, the largest near-impulsive burn achievable by the satellite is only around 0.3 m/s. Consequently, if the satellite is to be transferred to frozen orbit, the maneuver must be broken down into a sequence of small burns of no more than 0.3 m/s.

Figure 12 shows the resulting optimal transfer from an initial conditions of $e = 0.0025$ and $\omega = 311.9$ deg to the frozen conditions (Fig. 6), at $e = 0.0016$ and $\omega = 270$ deg: Each symbol corresponds to the orbital conditions produced by each 0.3-m/s burn, except for the last burn, which requires only 0.06 m/s. Figure 13 shows the same change but in $[e\cos\omega, e\sin\omega]$ coordinates. With the epicycle phase fixed according to Eq. (41), in the initial stage of firing the optimal approach mainly affects the eccentricity. In the later stage, as the frozen orbit insertion approaches completion, it is the argument of

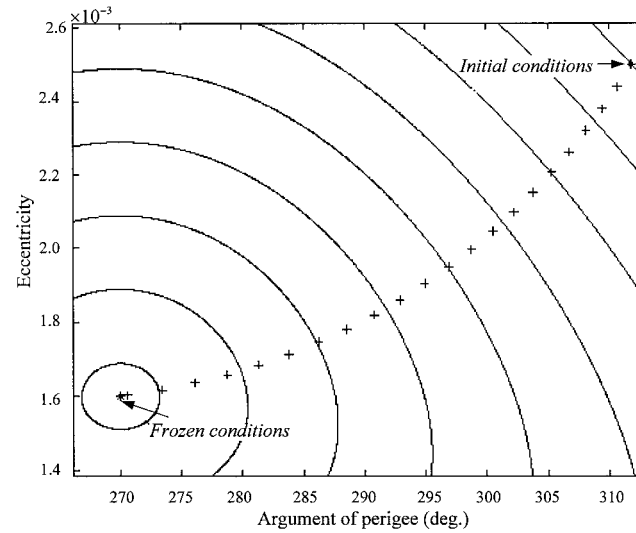

Fig. 12 Orientation of eccentricity and argument of perigee toward frozen conditions.

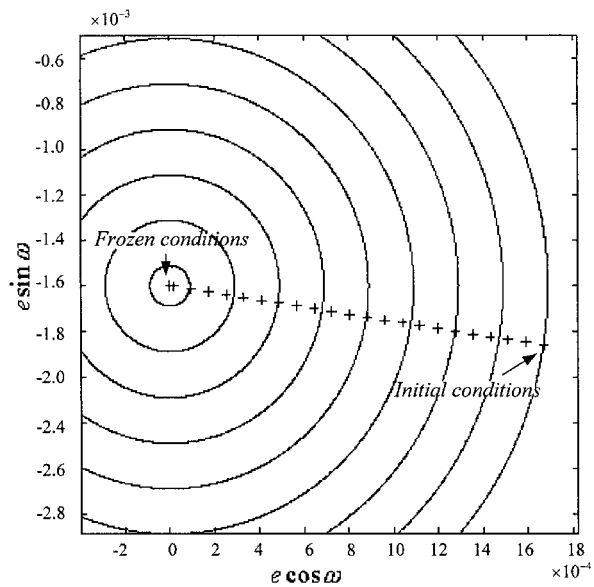

Fig. 13 Orientation of eccentricity and argument of perigee toward frozen conditions ($[e\cos\omega, e\sin\omega]$ coordinates).

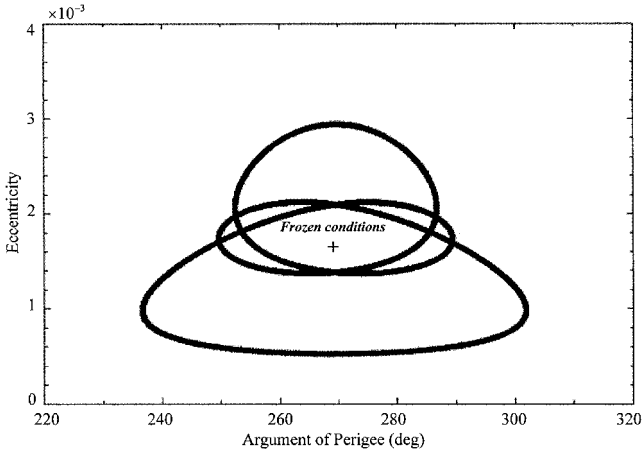

Fig. 14 Orientation of osculating eccentricity and argument of perigee of UoSAT-12 orbit after insertion into the frozen conditions of $e = 0.0016$ and $\omega = 270$ deg; zonal geopotential terms up to J_{36} included in numerical orbit integration.

perigee the changes most. The minimum delta-V requirement can be calculated from Eq. (32) to be 6.35 m/s. This is exactly the same as the total delta-V required for the multiburn strategy where the firing has been divided into 22 steps. Theoretically, the minimum time that the transfer process requires is 22 orbital revolutions, that is, the firing takes place every orbit at the same firing phase. In such a case, however, the spacecraft may require autonomous firing operation. The time between the consecutive firings can be extended according to the mission operation plan, and as shown in Eq. (32) and Fig. 9, the total delta-V requirement for the orbit transfer does not change.

Finally, Fig. 14 shows the variations in osculating eccentricity and argument of perigee after the orbit insertion stage. As a demonstration, the simulations are run for 3 years by using a precision orbit integrator.[18] The zonal geopotential terms up to J_{36} are included. It can be seen that, after the orbit insertion, neither secular nor long-period variations appear during the simulation period. The small rotations in e and ω around the frozen conditions are only due to the short-periodic perturbations.

Conclusions

We have analyzed the dynamics of frozen orbits through the epicycle element set. The frozen conditions can be found analytically with an arbitrary number of zonal harmonics included. We have shown that the minimum delta-V required for placing a satellite from arbitrary initial conditions into a frozen state does not depend on time. We have proposed the optimal strategy for frozen orbit transfer of low-thrust satellites. We use a series of small impulsive burns to shape the orbit step by step toward the frozen state. The firing phase is selected to minimize fuel usage. We have proven that, although the true anomaly is changing, the firing location is approximately fixed in inertial space for all burns, and the total delta-V required by this strategy is not greater than that required by the optimal single-burn strategy.

References

[1]Cutting, E., Born, G. H., and Frautnick, J. C., "Orbit Analysis For SEASAT-A," *Journal of the Astronautical Sciences*, Vol. 26, No. 4, 1978, pp. 315–342.

[2]Foister, J. W., "Frozen Orbit Analysis in the Martian System," M.S. Thesis, Air Force Inst. of Technology, Dec. 1987.

[3]Uphoff, C., "Orbit Design Concepts for Venus Orbiter," American Astronautical Society, Paper AAS-78-1437, Aug. 1978.

[4]d'Avanzo, P., Teofilatto, P., and Ulivieri, C., "Long-Term Effects on Lunar Orbiter," *Acta Astronautica*, Vol. 40, No. 1, 1997, pp. 13–20.

[5]Lara, M., Deprit, A., and Elipe, A., "Numerical Continuation of Families of Frozen Orbits in the Zonal Problem of Artificial Satellite Theory," *Celestial Mechanics and Dynamical Astronomy*, Vol. 62, 1995, pp. 167–181.

[6]Nickerson, K. G., Herder, R. W., Glass, A. B., and Cooley, J. L., "Application of Altitude Control Techniques for Low Altitude Earth Satellites," *Journal of the Astronautical Sciences*, Vol. 24, April–June 1978, pp. 129–148.

[7]Born, G. H., and Mitchell, J. L., "GEOSAT ERM Mission Design," *Journal of the Astronautical Sciences*, Vol. 36, Oct.–Dec. 1987, pp. 119–134.

[8]Smith, J. C., "Analysis and Application of Frozen Orbits for TOPEX Mission," AIAA Paper 86-2069, Aug. 1986.

[9]Vincent, M., "Eccentricity and Argument of Perigee Control for Orbits with Repeat Ground Tracks," American Astronautical Society, Paper AAS-91-516, Aug. 1991.

[10]Coffey, S., Deprit, A., and Deprit, E., "Paining Phase Spaces to Put Frozen Orbits in Context," American Astronautical Society, Paper AAS 91-427, Aug. 1991.

[11]Coffey, S., Deprit, A., and Deprit, E., "Frozen Orbits for Satellites Close to an Earth-like Planet," *Celestial Mechanics and Dynamics Astronomy*, Vol. 59, 1994, pp. 37–72.

[12]Cook, G. E., "Perturbations of Near-Circular Orbits by the Earth's Gravitational Potential," *Planet and Space Science*, Vol. 14, Jan. 1966, pp. 433–444.

[13]Bhat, R. S., Shapiro, B. E., and Frauenholz, R. B., "TOPEX/POSEIDON Orbit Acquisition Maneuver Sequence," *Advances in the Astronautical Sciences*, Vol. 85, Pt. 1, 1994, pp. 103–122.

[14]Bhat, R. S., Frauenholz, R. B., and Cannell, P. E., "TOPEX/Poseidon Orbit Maintenance Maneuver Design," *Advances in the Astronautical Sciences*, Vol. 71, Pt. 1, 1989, pp. 645–670.

[15]Jones, B., "Optimal Rendezvous in the Neighborhood of a Circular Orbit," *Journal of the Astronautical Sciences*, Vol. 24, No. 1, 1976, pp. 55–90.

[16]Fouquet, M., and Sweeting, M. N., "UoSAT-12 Minisatellite for High Performance Earth Observation at Low Cost," *Acta Astronautica*, Vol. 41, No. 3, 1996, pp. 173–182.

[17]Hashida, Y., and Palmer, P. L., "Epicycle Motion of Satellites About an Oblate Planet," *Journal of Guidance, Control, and Dynamics*, Vol. 24, No. 3, 2001, pp. 586–596.

[18]Palmer, P. L., Aarseth, S. J., Mikkola, S., and Hashida, Y., "High Precision Integration Methods for Orbit Modelling," *Journal of Astronautical Sciences*, Vol. 46, No. 4, 1998, pp. 329–342.